Loss of image quality in photobleaching during microscopic imaging of fluorescent probes bound to chromatin

Tytus Bernas
University of Silesia
Faculty of Biology and Protection of Environment
Department of Plant Anatomy and Cytology
Jagiellonska 28
Katowice, Poland
   and
Purdue University
Cytometry Laboratories
201 South University Street
West Lafayette, Indiana 47907

J. Paul Robinson
Purdue University
Cytometry Laboratories
201 South University Street
West Lafayette, Indiana 47907

Elikplimi K. Asem
Purdue University
School of Veterinary Medicine
625 Harrison Street
West Lafayette, Indiana 47907

Bartek Rajwa
Purdue University
Cytometry Laboratories
201 South University Street
West Lafayette, Indiana 47907

Abstract. Prolonged excitation of fluorescent probes leads eventually to loss of their capacity to emit light. A decrease in the number of detected photons reduces subsequently the resolving power of a fluorescence microscope. Adverse effects of fluorescence intensity loss on the quality of microscopic images of biological specimens have been recognized, but not determined quantitatively. We propose three human-independent methods of quality determination. These techniques require no reference images and are based on calculation of the actual resolution distance, information entropy, and signal-to-noise ratio (SNR). We apply the three measures to study the effect of photobleaching in cell nuclei stained with propidium iodide (PI) and chromomycin A3 (CA_3) and imaged with fluorescence confocal microscopy. We conclude that the relative loss of image quality is smaller than the corresponding decrease in fluorescence intensity. Furthermore, the extent of quality loss is related to the optical properties of the imaging system and the noise characteristics of the detector. We discuss the importance of these findings for optimal registration and compression of biological images. © 2005 Society of Photo-Optical Instrumentation Engineers. [DOI: 10.1117/1.2136313]

1 Introduction

Prolonged exposure to light can destroy the ability of a dye molecule to fluoresce. Photobleaching is a common phenomenon in light-microscopy imaging.[1] A decrease in fluorescence signal intensity of the observed specimen reduces the effective resolving power of a microscope, as demonstrated by theoretical models.[2–5] Hence, a low number of detected photons fundamentally limits applications of light microscopy.[6–9] Several strategies aimed at elimination of photobleaching or correction for this effect have been devised.[10–12] Nonetheless, the relationship between the fluorescence intensity of a specimen and the quality of its microscopic image has been established quantitatively only for simple objects of known structure, such as uniformly fluorescent beads[13,14] or subresolution particles.[15] Such data are scarce in the case of complex biological specimens.

Several measures of image quality have been proposed in the area of digital imaging and photography. Full-reference techniques rely on comparison of a given (distorted) image to a standard (undistorted) one, whereas half-reference methods model image structure for the purpose of such comparison.[16,17] However, owing to the presence of photonic noise, no microscopic image may be considered undistorted in the sense of these measures. Furthermore, construction of a model of an image of any biological structure appears to be problematic. Therefore, a no-reference image-quality estimator, which requires only a single image, must be used. Existing no-reference measures have been constructed to mimic the response of a human observer.[16,18–20] Thus, they may not be used to objectively determine the quality of microscopic images due to the limited availability of trained microscopists. In this work, we propose three human-independent methods of image-quality determination. We then apply these techniques to quantitatively investigate the adverse effects of photobleaching on the image quality.

2 Materials and Methods

2.1 Reagents

Ribonuclease A (RNase), propidium iodide (PI), chromomycin A3 (CA_3), and N-propyl gallate (NPG) were all from

Address all correspondence to Tytus Bernas, BMS, Purdue University, 201 S. University St., West Lafayette, IN 47907. Tel: 765–494–0757. Fax: 765–494–0517. E-mail: tytus@flowcyt.cyto.purdue.edu

Sigma-Aldrich (Poznan, Poland); formaldehyde [16% EM (electron microscopy) grade] was from Electron Microscopy Sciences (Fort Washington, Pennsylvania). Stocks of PI and CA_3 were made in phosphate-buffered saline (PBS) and kept at 4 °C; stocks of RNase were kept frozen. Compressed argon (99.998% pure) from BOC Gazy (Poland) was delivered to an imaged sample through copper and steel tubes.

2.2 Cell Culture and Labeling

MSU 1.1 human fibroblasts were cultured, fixed with formaldehyde, and treated using RNAse as described previously.[21] Nuclei of MSU 1.1 cells were stained by incubating 30 min with a solution of PI (5 μg/ml) or 25 min with CA_3 (100 μg/ml) in PBS. Following incubation with PI, the dye solution was removed and the preparation was incubated 45 min in fresh PBS prior to photobleaching. The rapid exchange of CA_3 ($t_{1/2}$ approximately 3 min) made it impossible to maintain a stable level of fluorescence in the absence of dye in the incubation solution. Thus, CA_3 was present in the sample throughout the experiment. Fluorescent labeling procedures and photobleaching experiments were carried out at room temperature. Cells incubated in PBS (without CA_3 or PI) were used to estimate contingent autofluorescence.

2.3 Confocal Microscopy

Fluorescence of PI (excitation 488 nm, emission 590 to 630 nm) or CA_3 (excitation 457 nm, emission 490 to 550 nm) and transmitted light (647 nm) were detected using a BioRad MRC1024 (Carl Zeiss Incorporated) confocal system equipped with a Nikon Diaphot 300 microscope, 60× PlanApo oil-immersion objective lens (NA 1.4), a 15-mW krypton-argon laser (ALC, Salt Lake City, Utah), and a 100-mW argon-ion laser (ILT, Salt Lake City, Utah). Time series of fluorescent confocal images of equatorial sections through nuclei (thickness of approximately 1.1 μm) were collected using alternately a low-intensity probing beam and a high-intensity bleaching beam. No measurable bleaching occurred when labels were excited using the probing beam alone. At the end of each time series, single transmitted-light images were registered. Images (512×512 pixels; 256 gray levels) were collected using LaserSharp 3.2 software (Carl Zeiss Incorporated). A final image was a sum of 20 (PI), 45 (CA_3), or 10 (transmitted light) consecutive scans. The number of scans was chosen so that the total number of detector counts at the onset of a photobleaching series was similar in the PI and CA_3 images and sufficient to fill the 8-bit dynamic range when images were registered using the probing beam. One should note that these two dyes have different absorption coefficients at their respective excitation wavelengths and different quantum efficiencies. Fluorescence in the control cells (incubated in the absence of PI or CA_3) was not detectable. Fluorescence was detected using photomultipliers in photon-counting (low signal) mode. Transmitted light was collected using the standard MRC1024 TLD detector. The intensity of excitation light was adjusted using neutral density filters.

2.4 Image Processing

2.4.1 Actual resolution distance

Performance of an optical imaging system is determined by its optical transfer function (OTF).[22] The modulus of the OTF
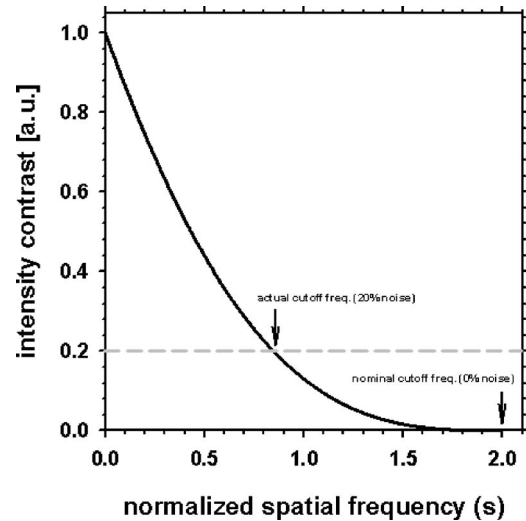

Fig. 1 Influence of noise on the cutoff frequency of the microscope MTF (continuous black line). The nominal cutoff frequency ($s=2$ in normalized optical units) is estimated in the absence of noise at zero contrast level. Frequency-independent noise (20%, gray dashed line) is introduced by imposing a lowest limit to the contrast. The practical cutoff frequency is calculated at the point where the MTF crosses this minimum contrast level.

(which is a complex function) characterizes the amplitude (maximum to minimum intensity contrast) of a spatial frequency transferred by the system. The OTF modulus [modulation transfer function (MTF)] of a confocal microscope used in further calculations is given (at the focal plane, *xy*) by an approximate formula[23]:

$$MTF(s) = 1 - 0.69s + 0.0076s^2 + 0.043s^3,$$

$$s = \frac{\lambda}{n \sin(\alpha)} f_r, \tag{1}$$

where λ is the emission wavelength; α is the objective aperture angle; f_r is the radial spatial frequency; s is the normalized f_r (expressed in optical units); and n is the light refraction coefficient.

The MTF intensity (representing contrast) is plotted versus the normalized spatial frequency (s) in Fig. 1. The resolution distance of the confocal microscope is determined by the maximum spatial frequency that can propagate through the system (i.e., the cutoff frequency f_c). In the absence of noise [or when the signal-to-noise ratio (SNR) is infinite], the cutoff frequency is the point at which the MTF crosses the zero-intensity contrast line (Fig. 1). Hence, the nominal (minimal) resolution distance (d) is achieved:

$$d = \frac{1}{f_c}$$

$$= 0.5 \frac{\lambda}{NA}$$

$$= 0.5 \frac{\lambda}{n \sin(\alpha)}, \tag{2}$$

where f_c is the cutoff frequency, and NA is the objective numerical aperture.

In practice, the effective intensity contrast in microscope images is reduced by noise. Consequently, the actual cutoff frequency is lower than the nominal.[4] This frequency was estimated from the intersection of the line determined by the noise-to-signal ratio (1/SNR, calculated as described further) and the MTF, as illustrated in Fig. 1.

The noise level was calculated using the algorithm described in Ref. 24. First, eight directional high-pass filters were applied to an image. The eight resulting images were added, and five pixels having the smallest sums were chosen to represent the most homogeneous image regions. The choice was restricted to the regions in which fluorescence intensity was at least 75% of the image maximum. The signal and noise were estimated using the following formulas:

$$S_W = \frac{\sum_{i,j \in W} I(i,j)}{N_W}$$

$$\sigma_W = \left\{ \frac{\sum_{i,j \in W} [I(i,j) - S_w]^2}{N_W} \right\}^{1/2}, \qquad (3)$$

where S_w is the average intensity (signal) in the region W; N_w is the number of pixels in the region; $I(i,j)$ is the intensity at the spatial coordinate (i,j); and σ_w is the standard deviation (noise) in the region W. Hence, the noise-to-signal ratio (1/SNR) was calculated using the formula[24]:

$$1/\text{SNR} = 1/\text{median}\left(\frac{S_w}{\sigma_W} \right), \qquad (4)$$

where SNR is the signal-to-noise ratio.

The ratio was used as an estimator of the minimum intensity contrast for a spatial frequency to propagate through the microscope. Hence, the actual cutoff frequency was determined at the point of intersection of the contrast line and the MTF, as illustrated in Fig. 1. The actual resolution distance (d) was then determined using Eq. (2) (f_c set to the the actual cutoff frequency) and plotted against average signal intensity calculated over the whole image using the formula:

$$I_{\text{avg}} = \frac{\sum_{i,j} I(i,j)}{N}$$

$$i,j \in \{I(i,j) > 0.75 \max[I(i,j)]\}, \qquad (5)$$

where I_{avg} is the average intensity in the regions where the intensity was at least 0.75 image maximum; and N is the number of pixels.

2.4.2 Relative information entropy

The information carried by a symbol in a discrete series was defined by Shannon[25] using information entropy:

$$H = -\sum_{i=1}^{n} p_i \log_2 p_i, \qquad (6)$$

where p_i is the probability of the occurrence of the i'th symbol; and n is a number of possible symbols.

The entropy of the information obtained using an imaging system was defined[26] using Fourier space representation of image data. For a discrete case, the entropy was defined using the formula:

$$H = -\sum_{f=0}^{f_c} P_f \log_2 P_f, \qquad (7)$$

where P_f is the relative energy of spatial frequency f, and f_c is the cutoff spatial frequency.

The entropy is maximal when the spatial frequencies have the same probability. In this case, the image is uniform with respect to brightness (intensity) and thus contains no distinct objects. Hence, relative entropy:

$$H_r = \frac{H}{H_{\max}} = \frac{\sum_{f=0}^{f_c} P_f \log_2 P_f}{\sum_{f=0}^{f_c} \frac{1}{n} \log_2 \frac{1}{n}}, \qquad (8)$$

where n is the number of frequency intervals, was used here to measure image quality. The entropy was plotted against the average fluorescence intensity calculated using:

$$I_{\text{avg}} = \frac{\sum_{i,j} I(i,j)}{N},$$

$$i,j \in \{I(i,j) > 15\} \qquad (9)$$

where I_{avg} is the average intensity in the regions where the intensity is greater than the background[15]; and N is the number of pixels.

2.4.3 Wavelet signal-to-noise ratio

The majority of the noise present in microscope images is caused by inherent variation in the arrival rate of photons due to the quantum nature of light. Thus, Poisson noise modeling[27] was combined with a bivariate wavelet shrinkage algorithm[28] to estimate changes of SNR in microscopic imaging. Average signal intensity was calculated from the resulting (denoised) images using Eq. (1) ($k=30$). The absolute difference between the denoised and the initial images was used as an estimate of the noise level, which was plotted against the average signal intensity. This intensity was linearly dependent on the number of photons detected by the photomultiplier. The respective proportionality coefficient (determined by the low-signal amplifier) was estimated to be 3.3. The expected noise was calculated for a given signal intensity using the Poisson model.

2.4.4 Photobleaching kinetics

Loss of fluorescence intensity was analyzed as described previously.[21] Briefly, the grayscale was subdivided into 25 consecutive intervals (i.e., from 6 to 15, 16 to 25, etc.) using
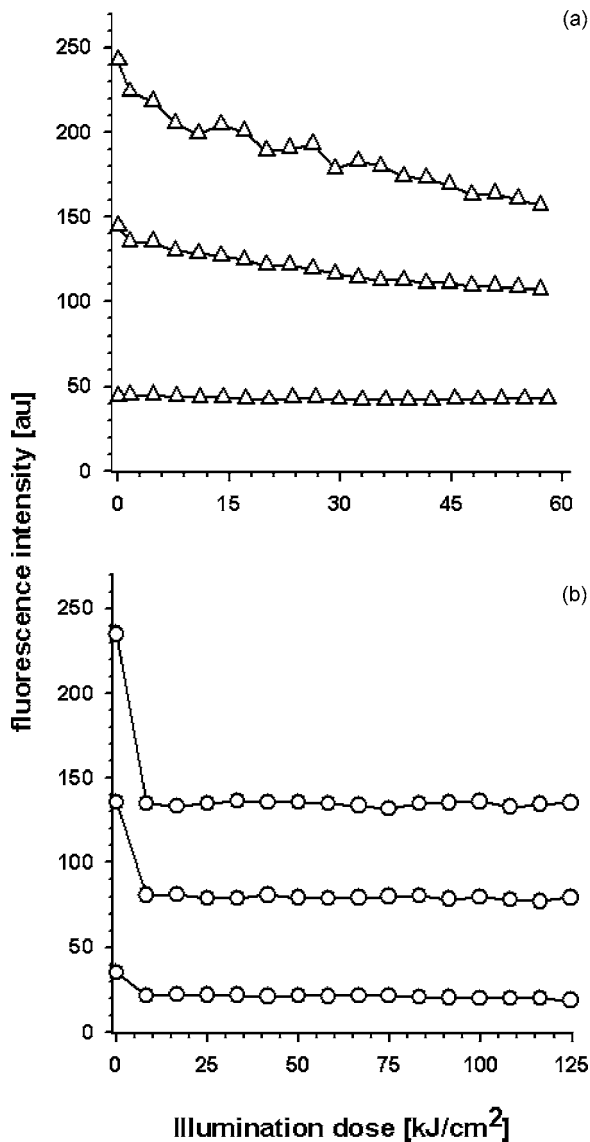
Fig. 2 Kinetics of photobleaching of PI [(a) triangles up] and CA$_3$ [(b), circles] bound to DNA. Equatorial sections of fixed cells were scanned with the laser in a confocal microscope. 20 (PI) or 45 (CA$_3$) successive scans were accumulated to form one image, and the average intensity (arbitrary units, au) of pixels of different initial brightness in images was plotted relative to the accumulated dose of incident light.

binary masks. Average intensities of pixels comprising each brightness class were calculated for each of the images in the stack before background (the mean intensity of signal in an area without cells, as determined from the transmitted light image) was subtracted. These corrected values were plotted against the total dose (J/cm^2) of the incident light and the number of scans (Fig. 2).

3 Results

3.1 Photobleaching Kinetics

Excitation of CA$_3$ and PI during fluorescence microscopy imaging of cell nuclei resulted in loss of fluorescence intensity of these dyes. Examples of the fluorescence-loss kinetic
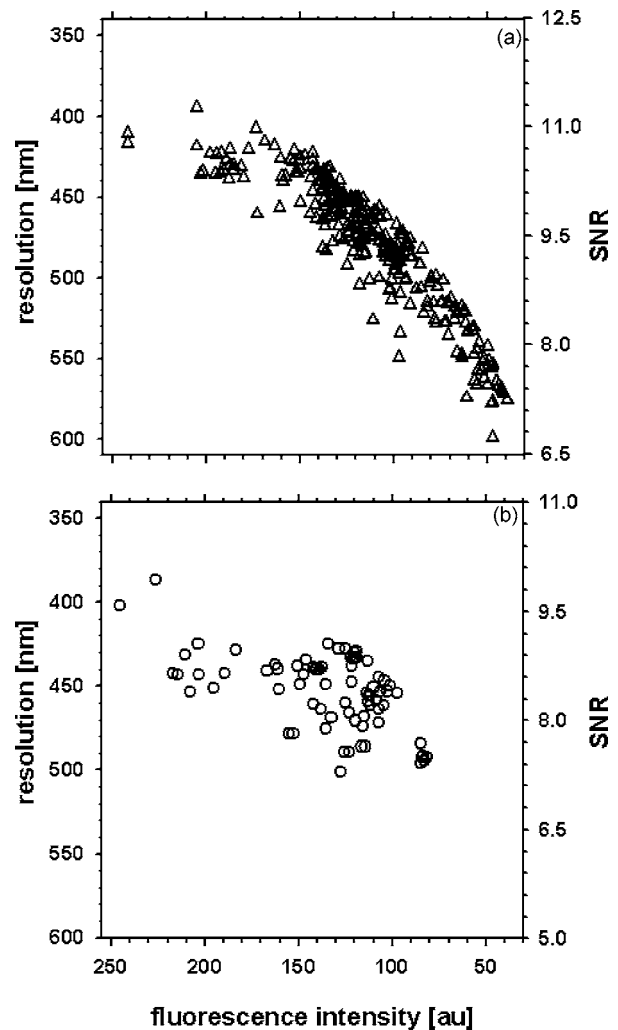

Fig. 3 Increase of actual resolution distance (left y axis) and decrease of SNR (right y axis) in photobleaching in images of nuclei stained with PI [(a), triangles up] and CA$_3$ [(b), circles]. Fluorescence intensity (x axis) represents the mean image brightness in the areas where SNR was calculated. Note that SNR values (represented on the linear scale) are approximates within ±2% error margin, owing to the fact that the MTF (and thus the actual resolution distance) is a nonlinear function of fluorescence intensity (see Materials and Methods in Sec. 2 and Fig. 1).

curves are shown in Fig. 2. The photobleaching rates were affected by excitation light flux and concentration of oxygen as described by Bernas et al.[21] We studied the influence of such fluorescence intensity loss on image quality. This parameter is assessed using the three measures discussed in the following paragraphs.

3.2 Increase of Actual Resolution Distance

Loss of fluorescence intensity due to photobleaching was followed by an increase in actual resolution distance of the images of cell nuclei stained with PI [Fig. 3(a)] and CA$_3$ [Fig. 3(b)]. This decrease for images registered with PI may be described using a square root function of average fluorescence intensity. No such inference could be made for CA$_3$ due to significant variation in the results. Nonetheless, the relative increase of resolution distance was significantly smaller than
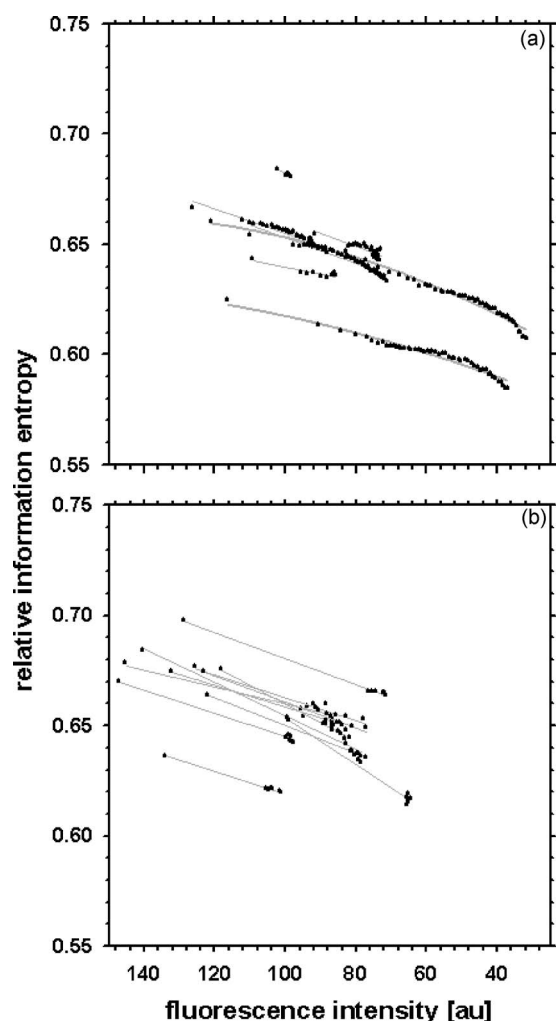
Fig. 4 Change of the relative information entropy in photobleaching of (a) PI and (b) CA$_3$ in cell nuclei. The individual images are depicted as black dots. Image series (each registered at a different region) are indicated with grey lines.

the corresponding decrease of fluorescence intensity for both fluorochromes. The actual resolution distance in the images registered using PI and CA$_3$ was similar. Furthermore, this actual resolution distance was significantly lower than the nominal for PI ($d=0.192$ μm) and CA$_3$ ($d=0.175$ μm) as well. One should note, however, that SNR in the former case was higher than in the latter.

3.3 Loss of Information

Photobleaching resulted in a loss of relative information entropy in the images of cell nuclei stained with PI [Fig. 4(a)] and CA$_3$ [Fig. 4(b)]. The entropy loss was proportional to the corresponding fluorescence decrease and similar for different image series (each registered at one field of view; see Materials and Methods in Sec. 2). Nonetheless, the entropy varied slightly from series to series. On the other hand, one should note that the entropy of the images of nuclei stained with PI and CA$_3$ is comparable for any given fluorescence level.

3.4 Decrease of Wavelet Signal-to-Noise Ratio

Loss of fluorescence intensity was also accompanied by a decrease of SNR estimated using wavelet shrinkage [Figs. 5(a) and 5(b)]. The SNR was similar for these two fluorochromes and was proportional to the square root of the fluorescence intensity. One should note, however, that the data variation was higher in the images registered using CA$_3$ [Fig. 5(a)], than in those using PI (Fig. 5(b)). The noise estimated with the wavelet shrinkage was lower than predicted from the number of detected photons and Poisson statistics [Figs. 5(c) and 5(d); see also Materials and Methods in Sec. 2]. This error increased slightly as the fluorescence intensity dropped.

3.5 Influence of Nominal Optical Resolution

One may hypothesize that the adverse effects of photobleaching on image quality (defined using the three proposed measures) are influenced by the size of the objects which may be resolved under ideal imaging conditions. For biological specimens, this parameter is determined by the nominal resolution distance of a microscope. Therefore, the effects of the intensity loss were studied using cell nuclei stained with PI and imaged with large ($d=0.360$ μm, NA$=0.75$) and small ($d=0.192$ μm, NA$=1.4$) resolution distance. The decrease in relative fluorescence intensity was followed by a loss in relative image quality measured using the actual resolution distance [Fig. 6(a)], information entropy [Fig. 6(b)], and wavelet SNR [Fig. 6(c)]. The impact of photobleaching on the actual resolution distance was greater for the low-NA objective than for the high-NA objective. A similar pattern was found for information entropy. The decrease of wavelet SNR was, however, similar for images registered with small and large nominal resolution distance.

4 Discussion

4.1 Actual Resolution Distance

The relative increase of the actual resolution distance was significantly lower than the corresponding change in fluorescence of CA$_3$ and PI. Since the resolution distance was nearly proportional to the SNR, it seems plausible that the noise was dependent on the signal in a nonlinear manner. The resolution distance could be described using the square-root function of PI fluorescence intensity. Thus, one may hypothesize that the majority of the noise obeyed Poisson statistics. The images of nuclei stained with CA$_3$ and PI were registered using a similar number of photons. Thus, one might expect smaller actual resolution distance in the former, as CA$_3$ was excited at and fluoresced at a shorter wavelength than PI. However, no such difference in actual resolution distance was observed. It should be noted that images of CA$_3$ fluorescence were constructed from 45 summed scans, whereas only 20 were accumulated for PI (see Materials and Methods in Sec. 2). Consequently, it is likely that detector noise was higher in CA$_3$ images than in PI images. The higher variability of the points in the CA$_3$ plot [compare Figs. 3(a) and 3(b)] is in agreement with this hypothesis.

4.2 Information Entropy

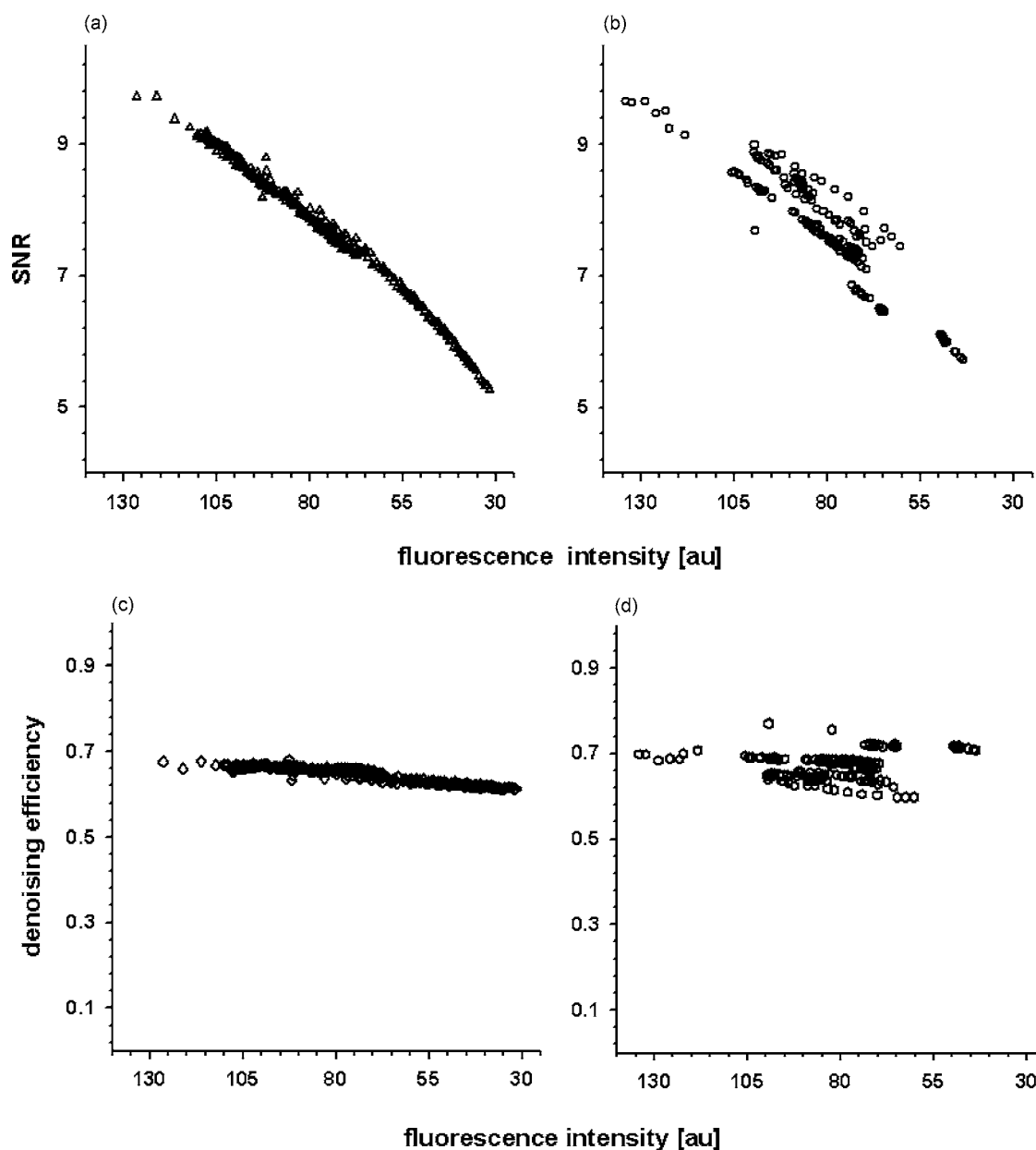The relative decrease in entropy was very low compared to the corresponding loss of fluorescence intensity of CA$_3$ and

Fig. 5 Decrease in SNR in the images of nuclei labeled using (a) PI and (b) CA$_3$ as estimated using the wavelet shrinkage algorithm. The noise expressed as the fraction of the theoretical value is plotted against the respective fluorescence intensity for (c) PI and (d) CA$_3$.

PI. Therefore, one may postulate that only a small information loss occurred due to photobleaching. Hence, it seems possible to restore a faded image efficiently by correcting for photobleaching, provided that the kinetics of this process is well characterized. An example of such restoration is demonstrated in Fig. 7. The images of PI and CA$_3$ fluorescence were characterized by similar values of information entropy. However, one may note differences in initial entropy between different series of images (experiments) registered using the same flurochrome (i.e., CA$_3$ or PI). This is not surprising as the entropy is calculated in the frequency (Fourier) domain, and the spectrum depends on the number of nuclei in the image. It would be reasonable to assume that the information content increased with the number of acquisitions of relevant objects (nuclei, in this case).

4.3 Wavelet Signal-to-Noise Ratio

The wavelet SNR followed a square-root dependence on fluorescence intensity in a pattern similar to that of the actual resolution distance. However, the SNR values estimated using the wavelet algorithm are higher (lower noise) than the values obtained using the spatial domain method (see Materials and Methods in Sec. 2). While the former method estimates only Poisson noise, the latter gives the total value. On the other hand, the SNR in the wavelet domain is calculated using all the pixels, whereas only a fraction of the pixels is used for calculations in the spatial domain (see Materials and Methods in Sec. 2). Therefore, the wavelet-based algorithm is more precise from a statistical point of view. This notion is in agreement with the fact that the SNR obtained with this
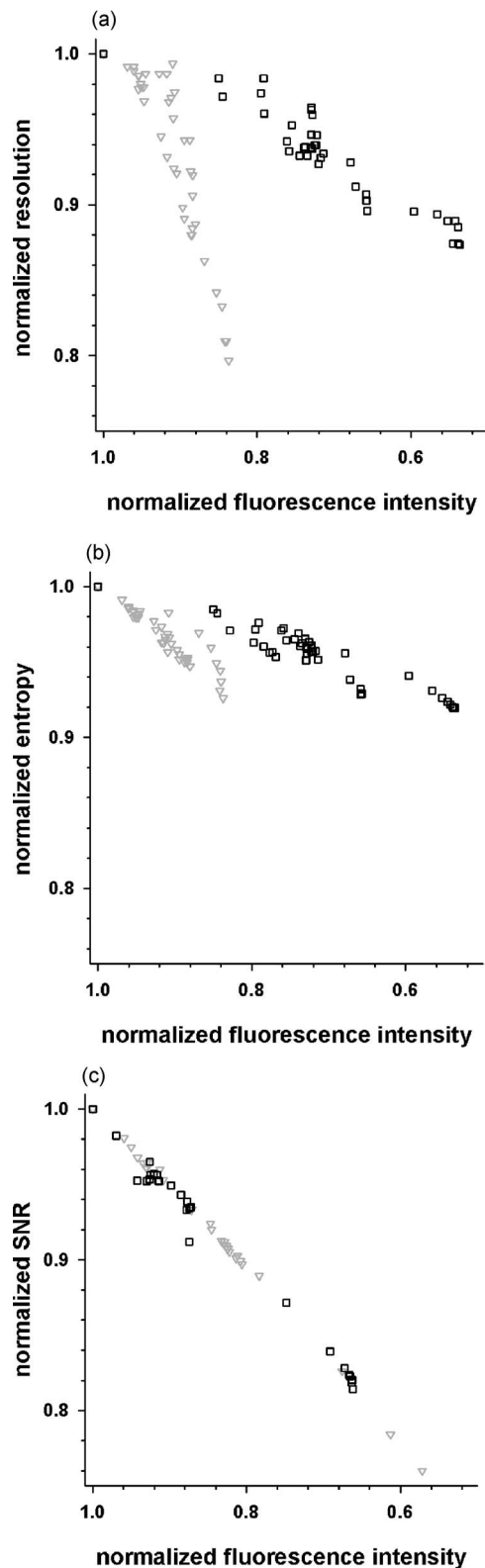
Fig. 7 Structural information preservation in photobleaching of PI-stained nuclei: (a) initial (nonbleached) image, (b) image after bleaching, (c) corrected (bleached) image, and (d) the difference between the corrected and the initial image.

method exhibited smaller variability compared to the SNR computed in the spatial domain.

4.4 *Influence of Nominal Optical Resolution*

The relationship between the image quality and the number of registered fluorescence photons was affected by the nominal optical resolution of the microscope. The calculation of actual resolution distance depends on the MTF shape (in particular the cutoff frequency; see Materials and Methods in Sec. 2). Thus, it seems reasonable that a similar drop in SNR would result in a more pronounced increase of the actual resolution distance in the case of low NA (more steep MTF, see Fig. 1) compared with high NA (less steep MTF). The decrease in SNR narrows the range of spatial frequencies that contribute to the imaged structure of the nuclei. As with the actual resolution distance, the photobleaching caused a greater loss of information entropy in the images registered with large nominal resolution distance in comparison to these registered with small distance. On the other hand, the wavelet SNR is computed on a pixel-to-pixel basis and therefore was not affected by the optical properties of the imaging system. Hence, the effect of photobleaching measured using this method is similar for images registered with small and large nominal resolution distance. An overview of variables affecting the three quality measures is given in Table 1.

4.5 *Autofluorescence and Image Quality*

No signal was detected if the cells were not labeled with PI or CA_3, indicating that endogenous fluorescence (autofluorescence) did not interfere with image registration in our experiments. Therefore, one may assume that the same biological structure (fluorescently labeled chromatin) was registered at the onset and at the end of photobleaching. In other words, the subsequent images of the same field of view differed with

Fig. 6 Effect of photobleaching on the quality of images of nuclei stained with PI and registered with low (gray triangles) and high (black squares) nominal resolution. The quality was estimated using (a) the actual resolution distance, (b) entropy, and (c) wavelet SNR. These parameters are expressed as fractions of the respective values for the nonbleached images. Similarly, the fluorescence intensities were normalized to the respective values for the initial (nonbleached) images.
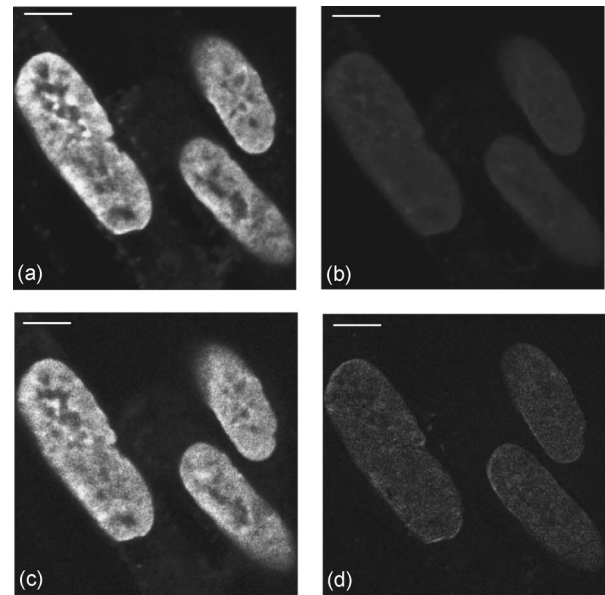
Table 1 Overview of variables influencing the three image-quality measures: actual resolution, information entropy, and wavelet SNR.

	Actual resolution	Information entropy	Wavelet SNR
Assumed noise distribution	Any (spatially uncorrelated)	Any	Poisson (photonic)
Dependence on the nominal resolution distance	Yes	Yes	No
Dependence on the fluorescence spatial distribution (image content)	No	Yes	No
Dependence on the fluorescence intensity distribution (histogram)	No (affected only by maximum detected intensity)	Yes	Yes (SNR is an average weighted by the intensity distribution)

respect to the total number of detected photons but not the subcellular fluorescence distribution. However, autofluorescence of biological specimens is not always negligible. Possible sources of autofluorescence include endogenous fluorophores, such as flavins and flavoproteins,[29,30] lipopigments and phospholipids,[31,32] or putative endogenous Schiff-base compounds.[33,34] Another source of nonspecific fluorescence signal might lie in the fixation procedure itself.[35,36] The presence of autofluorescence may reduce the effective dynamic range of the light detector available for registration of specific fluorescence signal. Consequently, the presence of autofluorescence can be a precision-limiting factor in the measurement of concentration (amount) of a fluorophore of interest. Moreover, if autofluorescence is nonuniform within a cell, it can obscure cellular distribution of the specific fluorescent label. To the authors' knowledge, no detailed studies of the photobleaching kinetics of compounds that contribute to autofluorescence have been reported. However, one may expect that differences in photobleaching kinetics between the endogenous fluorochromes and exogenous fluorescent labels could further complicate microscopic imaging. If such differences occur, the intensity ratio between the autofluorescence and the specific fluorescence would depend on the intensity of excitation light and the image registration time. Consequently, spatial distribution of total cell fluorescence could change in the course of imaging due to different photobleaching of the autofluorescence and the specific fluorescence. Since autofluorescence did not contribute to the signal in our experiments, image quality was a monotonic (and smooth) function of fluorescence intensity. However, if the distribution of the total fluorescence changed in the course of sample illumination, the image quality might not depend on the fluorescence intensity in monotonic fashion.

4.6 Practical Applications

The quality measures proposed here make it possible to estimate the fundamental limits of measurement precision in the spatial and intensity domains. Hence, using these measures one may establish reliability of measurement of a given concentration of fluorophore (and thus the labeled molecule of interest). Furthermore, the reliability of detection of an object

of a given size (and thus precision of structural studies) may be verified as well. To summarize, using these quality measures one may estimate the amount of syntactic information present in biological images. However, it is up to the researcher to decide whether the spatial distribution of fluorescence registered with a microscope conveys any biological information. Thus, the suitability of a quality measure depends on the semantic information to be extracted from an image. In other words, the choice of the proper measure is a function of the biological question to be answered.

Utility of the proposed quality measures may be extended beyond image analysis. The following notions indicate some image-processing applications.
• The observed decrease of image quality was smaller than the corresponding loss of fluorescence intensity as estimated using the three algorithms proposed here. Hence, efficient restoration of faded fluorescence images may be possible if the photobleaching kinetics are known.[11,21]
• One should note that the quality of the images studied here was well below the maximum, even when no photobleaching occurred. Therefore, it seems plausible to implement efficient compression schemes using appropriate denoising procedures.

References

1. R. Y. Tsien and A. Waggoner, "Fluorophores for confocal microscopy. Photophysics and photochemistry," in *Handbook of Biological Confocal Microscopy*, J. B. Pawley, Ed., pp. 267–279, Plenum Press, New York (1995).
2. A. van den Bos, "Optical resolution: an analysis based on catastrophe theory," *J. Opt. Soc. Am. A* **4**, 1402–1406 (1987).
3. A. Van Den Bos and A. J. Den Dekker, "Coherent model-based optical resolution," *J. Opt. Soc. Am. A Opt. Image Sci. Vis* **13**, 1667–1669 (1996).
4. E. H. K. Stelzer, "Contrast, resolution, pixelation, dynamic range and signal to noise ratio: fundamental limits to resolution in fluorescence light microscopy," *J. Microsc.* **189**, 15–24 (1998).
5. M. Shahram and P. Milanfar, "Imaging below the diffraction limit: a statistical analysis," *IEEE Trans. Image Process.* **13**, 677–689 (2004).
6. V. E. Centonze and J. G. White, "Multiphoton excitation provides optical sections from deeper within scattering specimens than confocal imaging," *Biophys. J.* **75**, 2015–2024 (1998).
7. J. M. Girkin, A. I. Ferguson, D. L. Wokosin, and A. M. Gurney, "Confocal microscopy using an InGaN violet laser diode at 406 nm," *Opt. Express* **7**, 336–341 (2000).

8. S. P. Schilders and M. Gu, "Limiting factors on image quality in imaging through turbid media under single-photon and two-photon excitation," *Microsc. Microanal.* **6**, 156–160 (2000).

9. I. T. Young, "Quantitative microscopy," *IEEE Eng. Med. Biol. Mag.* **15**, 59–66 (1996).

10. R. A. Abuknesha, H. M. al-Mazeedi, and R. G. Price, "Reduction of the rate of fluorescence decay of fitc-and carboxyfluorescein-stained cells by anti-fitc antibodies," *Histochem. J.* **24**, 73–77 (1992).

11. T. A. Nagelhus, G. Slupphaug, H. E. Krokan, and T. Lindmo, "Fading correction for fluorescence quantitation in confocal microscopy," *Cytometry* **23**, 187–195 (1996).

12. K. Tanhuanpaa, J. Virtanen, and P. Somerharju, "Fluorescence imaging of pyrene-labeled lipids in living cells," *Biochim. Biophys. Acta* **1497**, 308–320 (2000).

13. R. M. Zucker and O. Price, "Evaluation of confocal microscopy system performance," *Cytometry* **44**, 273–294 (2001).

14. R. M. Zucker and O. T. Price, "Statistical evaluation of confocal microscopy images," *Cytometry* **44**, 295–308 (2001).

15. A. Santos and I. T. Young, "Model-based resolution: applying the theory in quantitative microscopy," *Appl. Opt.* **39**, 2948–2958 (2000).

16. Z. Wang, A. C. Bovik, H. R. Sheikh, and E. P. Simoncelli, "Image quality assessment: from error visibility to structural similarity," *IEEE Trans. Image Process.* **13**, 600–612 (2004).

17. Z. Wang, E. P. Simoncelli, and A. C. Bovik, "Multiscale structural similarity for image quality assessment," *Conf. Record 37th Asilomar Conf. Signals, Syst. Computers* **2**, 1398–1402 (2003).

18. Z. Wang, L. Lu, and A. C. Bovik, "Video quality assessment based on structural distortion measurement," *Signal Process. Image Commun.* **19**, 121–132 (2004).

19. Z. Wang, A. R. Sheikh, and A. C. Bovik, "Objective video quality assessment," in *The Handbook of Video Databases: Design and Applications*, B. Furht and O. Marqure, Eds., pp. 1041–1078, CRC Press, New York (2003).

20. H. R. Sheikh, Z. Wang, L. Cormack, and A. C. Bovik, "Blind quality assessment for Jpeg2000 compressed images," *IEEE Asilomar Conf. Signals, Syst. Computers* **2**, 2069–2072 (2002).

21. T. Bernas, M. Zarebski, P. R. Cook, and J. W. Dobrucki, "Minimizing photobleaching during confocal microscopy of fluorescent probes bound to chromatin: role of anoxia and photon flux," *J. Microsc.* **215**, 281–296 (2004).

22. J. B. Pawley, *Handbook of Biological Confocal Microscopy*, Plenum Press, New York (1995).

23. P. Stokseth, "Properties of a defocused optical systems," *J. Opt. Soc. Am.* **59**, 1314–1421 (1969).

24. A. Amer, E. Dubois, and A. Mitiche, "Reliable and fast structure-oriented video noise estimation," IEEE Intl. Conf. Image Process. **1**, 840–843 (2002).

25. C. E. Shannon, "A mathematical theory of communication," *Bell Syst. Tech. J.* **25**, 379–423 (1948); **25**, 623–656 (1948).

26. E. L. O'Neil and T. Asakura, "Optical image formations in terms of entropy transformations," *J. Phys. Soc. Jpn.* **16**, 172–177 (1961).

27. R. Nowak and R. G. Baraniuk, "Wavelet domain filter for photon imaging systems," *IEEE Trans. Image Process.* **8**, 1–24 (1999).

28. L. Sendur and I. W. Selesnick, "Bivariate image shrinkage with local variance estimation," *IEEE Trans. Signal Process.* **50**, 2744–2756 (2002).

29. S. Huang, A. A. Heikal, and W. W. Webb, "Two-photon fluorescence spectroscopy and microscopy of NAD(P)H and flavoprotein," *Biophys. J.* **82**, 2811–2825 (2002).

30. J. V. Rocheleau, W. S. Head, and D. W. Piston, "Quantitative NAD(P)H/flavoprotein autofluorescence imaging reveals metabolic mechanisms of pancreatic islet pyruvate response," *J. Biol. Chem.* **279**, 31780–31787 (2004).

31. N. Billinton and A. W. Knight, "Seeing the wood through the trees: a review of techniques for distinguishing green fluorescent protein from endogenous autofluorescence," *Anal. Biochem.* **291**, 175–197 (2001).

32. A. C. Croce, A. Ferrigno, M. Vairetti, R. Bertone, I. Freitas, and G. Bottiroli, "Autofluorescence properties of isolated rat hepatocytes under different metabolic conditions," *Photochem. Photobiol. Sci.* **3**, 920–926 (2004).

33. H. Andersson, T. Baechi, M. Hoechl, and C. Richter, "Autofluorescence of living cells," *J. Microsc.* **191**, 1–7 (1998).

34. M. Dellinger, M. Geze, R. Santus, E. Kohen, C. Kohen, J. G. Hirschberg, and M. Monti, "Imaging of cells by autofluorescence: a new tool in the probing of biopharmaceutical effects at the intracellular level," *Biotechnol. Appl. Biochem.* **28**, 25–32 (1998).

35. J. A. Steinkamp, N. M. Lehnert, J. F. Keij, and B. E. Lehnert, "Enhanced immunofluorescence measurement resolution of surface antigens on highly autofluorescent, glutaraldehyde-fixed cells analyzed by phase-sensitive flow cytometry," *Cytometry* **37**, 275–283 (1999).

36. P. Tagliaferro, C. J. Tandler, A. J. Ramos, J. Pecci Saavedra, and A. Brusco, "Immunofluorescence and glutaraldehyde fixation. A new procedure based on the Schiff-quenching method," *J. Neurosci. Methods* **77**, 191–197 (1997).